MAGNETISM

# Proximate deconfined quantum critical point in $SrCu_2(BO_3)_2$

Yi Cui[1]†, Lu Liu[2,3]†, Huihang Lin[1]†, Kai-Hsin Wu[4], Wenshan Hong[2], Xuefei Liu[1], Cong Li[1], Ze Hu[1], Ning Xi[1], Shiliang Li[2,5,6], Rong Yu[1,7]*, Anders W. Sandvik[4,2]*, Weiqiang Yu[1,7]*

The deconfined quantum critical point (DQCP) represents a paradigm shift in quantum matter studies, presenting a "beyond Landau" scenario for order-order transitions. Its experimental realization, however, has remained elusive. Using high-pressure $^{11}B$ nuclear magnetic resonance measurements on the quantum magnet $SrCu_2(BO_3)_2$, we here demonstrate a magnetic field–induced plaquette singlet to antiferromagnetic transition above 1.8 gigapascals at a notably low temperature, $T_c \simeq 0.07$ kelvin. First-order signatures of the transition weaken with increasing pressure, and we observe quantum critical scaling at the highest pressure, 2.4 gigapascals. Supported by model calculations, we suggest that these observations can be explained by a proximate DQCP inducing critical quantum fluctuations and emergent O(3) symmetry of the order parameters. Our findings offer a concrete experimental platform for investigation of the DQCP.

The theoretically proposed deconfined quantum critical point (DQCP) (*1*) connects two different ordered ground states of quantum matter by a continuous quantum phase transition (QPT). This type of criticality, which has been explored primarily in the context of two-dimensional (2D) quantum magnets (*2*), lies beyond the conventional paradigm of discontinuous (first-order) transitions between ordered phases with unrelated symmetries. The DQCP is associated with unconventional phenomena, including fractional spinon excitations and deconfined gauge fluctuations (*3*–*5*). Further investigations have extended the concept, introducing emergent symmetries (*6*–*11*) and exotic first-order transitions (*12*, *13*). In a very recent scenario, the DQCP is proposed to be a multicritical point (*14*, *15*) connected to a gapless quantum spin liquid (QSL) (*16*–*20*).

Although DQCP phenomena are broadly relevant in quantum materials (*21*), there has been no supportive experimental identification in any system. Quantum magnets in which the interactions can be varied over a wide enough range to realize two phases bordering a DQCP are rare. An exception is the layered material $SrCu_2(BO_3)_2$ (*22*–*24*), in which antiferromagnetic (AFM) Heisenberg interactions between the $S = 1/2$ $Cu^{2+}$ spins (Fig. 1A) provide a faithful realization of the 2D Shastry-Sutherland model (SSM) (*25*). In the SSM, three different $T = 0$ phases are well established to form as a function of the ratio $g = J/J'$ of the inter- to intradimer couplings (*26*, *27*): an exact dimer-singlet phase (DS, with singlets on the $J'$ bonds), a twofold degenerate plaquette-singlet (PS) phase (Fig. 1B), and a Néel AFM phase (Fig. 1C). At ambient pressure, $SrCu_2(BO_3)_2$ is well described by the $g \simeq 0.63$ SSM with a DS ground state (*24*). An applied pressure increases $g$, driving the system into a PS phase at $P \simeq 1.8$ GPa (*28*, *29*), which persists with transition temperature $T_P \simeq 2$ K up to $P \simeq 2.6$ GPa (*30*, *31*). An AFM phase with Néel temperature $T_N$ from 2.5 to 4 K has been detected between 3.2 and 4 GPa (*30*).

Here, we report a $^{11}B$ nuclear magnetic resonance (NMR) study of $SrCu_2(BO_3)_2$ in a magnetic field $H$ up to 15 T and at pressures up to 2.4 GPa, aiming to characterize the field-driven PS-AFM transition. At 2.1 GPa, PS and AFM transitions are resolved using their NMR signatures and merge at a common point ($H_C$,$T_C$), with $H_C \simeq 6$ T and $T_C \simeq 0.07$ K (Fig. 1D). Such a low $T_C$ in relation to $T_P$ and $T_N$ farther away from $H_C$ indicates proximity to a $T_C = 0$ QPT. First-order discontinuities at ($H_C$,$T_C$) weaken with increasing pressure, and we observed quantum-critical scaling of the spin-lattice relaxation at 2.4 GPa for $T > T_C$.

Our results support the existence of a multicritical DQCP controlling the quantum fluctuations at 2.4 GPa, with $T_C$ on the associated first-order line suppressed by an emergent O(3) symmetry of the combined scalar PS and O(2) AFM order parameters (*7*, *8*). By synthesizing past and present experiments on $SrCu_2(BO_3)_2$ and model calculations, we arrived at the global phase diagram depicted in Fig. 2. Before further discussing the DQCP scenario, we present our NMR detection of the various phases and transitions.

## NMR identification of phases

We performed $^{11}B$ NMR measurements on $SrCu_2(BO_3)_2$ single crystals at pressures of up to 2.4 GPa in fields between 0.2 and 15 T and temperatures down to 0.07 K. Experimental details are provided in the supplementary materials (*33*). We first discuss NMR line shifts to detect the relevant quantum phases and transitions, followed by results of the spin-lattice relaxation rate $1/T_1$.

A typical $^{11}B$ NMR spectrum, shown in Fig. 3A, has a central peak with four satellite peaks on either side, from inequivalent sites B1 to B4 (Fig. 1A) caused by a small tilt angle between the field and the crystalline $c$ axis (*33*). The satellites are sensitive to changes of the lattice structure because of the local coupling between the nuclear quadrupole moment and the electric field gradient (*33*). As shown at a low field and $P = 2.1$ GPa in Fig. 3B, the full-width at half maximum (FWHM) height of the satellites increases on cooling <10 K until a maximum at $T \simeq 3$ K, reflecting increasing lattice fluctuations when the spins form fluctuating plaquette singlets above the ordered PS phase (*31*). This PS liquid crosses over to the trivial paramagnetic (PM) state at higher temperature.

Below 1.8 K, the FWHM in Fig. 3B rises sharply and saturates around 1 K. As explained in section S2 of the supplementary materials (*33*), the rapid broadening follows from an orthogonal lattice distortion when a full-plaquette (FP) PS state (Fig. 1B) forms. The FWHM as a proxy for the PS order parameter is further corroborated by the consistency of $T_P \simeq 1.8$ K at the low field applied in Fig. 3B with the location of a sharp specific-heat peak (*30*, *31*), marked in Fig. 1D.

Figure 3C shows the evolution of the central peak with $T$ at $P = 0.9$ GPa and $H = 4$ T. The negative Knight shift at the higher temperatures reflects the hyperfine coupling $A_{hf} \simeq -0.259\ T/\mu_B$ [see section S3 of the supplementary materials (*33*)] for $H \| c$ (*34*, *35*). The shift increases rapidly below $T^* \simeq 7$ K when dimer singlets form in the DS state. At 2.1 GPa (Fig. 3E), PS order forms < 2 K, but the Knight shift changes rapidly at $T \simeq 4$ K when the PS liquid forms.

The first-order transition between the DS phase and the PS or PS liquid phase terminates at an Ising-type critical point, which at $H = 0$ is located at $P \simeq 1.9$ GPa, $T \simeq 3.3$ K (*31*). At low $T$, the DS-PS transition takes place between 1.7 and 1.8 GPa (*30*). The first-order DS line must therefore bend slightly, as indicated in Fig. 2A, and can be crossed versus $T$ at fixed $P$ and $H$. Indeed, at 1.85 GPa (Fig. 3D),

[1]Department of Physics and Beijing Key Laboratory of Optoelectronic Functional Materials and Micro-nano Devices, Renmin University of China, Beijing 100872, China. [2]Beijing National Laboratory for Condensed Matter Physics and Institute of Physics, Chinese Academy of Sciences, Beijing 100190, China. [3]School of Physics, Beijing Institute of Technology, Beijing 100081, China. [4]Department of Physics, Boston University, Boston, MA 02215, USA. [5]School of Physical Sciences, Graduate University of the Chinese Academy of Sciences, Beijing 100190, China. [6]Songshan Lake Materials Laboratory, Dongguan, Guangdong 523808, China. [7]Key Laboratory of Quantum State Construction and Manipulation (Ministry of Education), Renmin University of China, Beijing 100872, China.
*Corresponding author. Email: rong.yu@ruc.edu.cn (R.Y.); sandvik@bu.edu (A.W.S.); wqyu_phy@ruc.edu.cn (W.Y.)
†These authors contributed equally to this work.

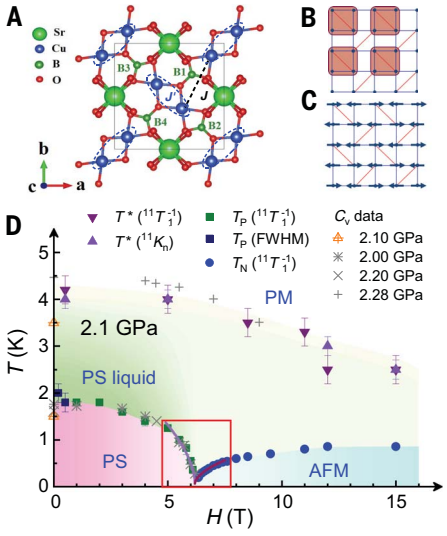


**Fig. 1. Experimental overview.** (**A**) Atomic structure of a $SrCu_2(BO_3)_2$ plane. Pairs of $Cu^{2+}$ ions form spin dimers (ellipses) with Heisenberg intradimer ($J'$) and interdimer ($J$) interactions (black dashed line). Each unit cell contains four B ions, for which we investigated the NMR response. (**B**) The PS phase in the equivalent square lattice of $J$ (blue) and $J'$ bonds (red). In $SrCu_2(BO_3)_2$, the singlets (shading) form on the full ($J'$) plaquettes in one of two symmetry-equivalent patterns, whereas in the SSM, the singlets form on half of the empty plaquettes. (**C**) The AFM phase, which breaks O(3) symmetry when $H = 0$ and O(2) symmetry when $H \neq 0$. For $SrCu_2(BO_3)_2$ in a $c$-axis field, we found that the moments ordered along the $a$ or $b$ axis. (**D**) Field-temperature phase diagram at 2.1 GPa, showing the PM, PS liquid, ordered PS, and AFM phases resolved by our NMR measurements (Figs. 3 to 5). The transition temperatures $T_P$ and $T_N$ and the crossover temperature $T^*$ are compared with specific-heat measurements (*30*, *31*). The data for 2.1 GPa come from (*30*) and the rest from (*31*). The red box marks the regime analyzed in Fig. 5F.

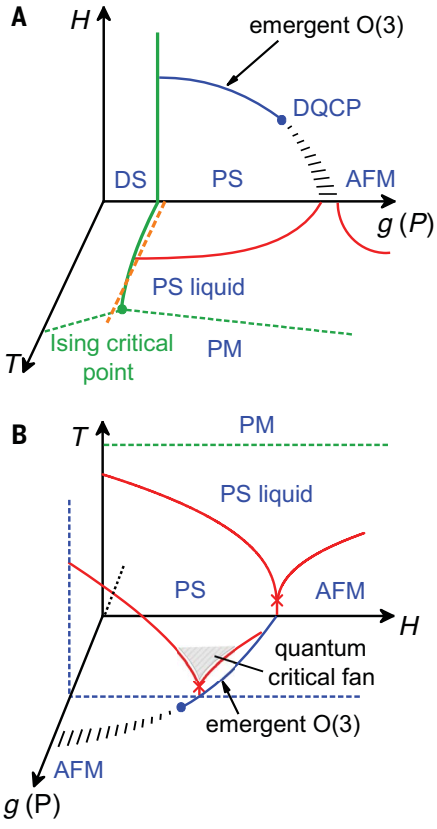


**Fig. 2. Schematic phase diagram and DQCP scenario.** (**A**) Phases in the space of coupling [$g = J/J'$ in the SSM, $P$ in $SrCu_2(BO_3)_2$], temperature, and magnetic field. A multicritical DQCP separates a line of first-order QPTs and either a QSL phase (*17*) or a line of generic DQCPs (*38*); the region marked with dashed lines represents this undetermined feature. The first-order DS transition at fixed $H$ (solid green line) terminates at an Ising critical point [green circle, based on previous experiments (*31*)]. The green dashed lines indicate crossovers at $T^*(g)$ into the PM phase. The dashed orange line shows how the slightly curved first-order DS transition line can be crossed versus $T$ at fixed $P$ (based on present experimental data). The ordered AFM phase at $T > 0$ requires interlayer couplings, as in $SrCu_2(BO_3)_2$. The magnetization plateau states at larger $H$ (*28*, *32*) are not shown. (**B**) Phase diagram drawn to highlight ($H$,$T$) planes exemplified by Fig. 1D. Red crosses indicate $T_C > 0$ caused by weak 3D effects and violations of O(3) symmetry. The shading represents the "fan" in which quantum critical scaling is expected (supported by present experimental data). The blue dashed lines indicate the plane of highest-pressure (2.4 GPa) measurements.

the central peak is split at temperatures between 3 and 4 K, indicating phase coexistence. Previously, a different splitting was reported at 2.4 GPa (*35*, *36*), which was perhaps caused by pressure inhomogeneity, but we observed the double peak only at 1.85 and 1.95 GPa [see section S3 of the supplementary materials (*33*)]. Outside of this pressure range, $T^*$ likely only marks a rapid crossover between the PM and PS liquid, with associated sharp specific heat peaks (*30*, *31*) which were observed also away from the critical point and reproduced (*31*) by SSM calculations. We have found no NMR signatures of a structural transition here or at higher temperatures [see section S3 of the supplementary materials (*33*)].

Above 1.95 GPa, AFM order emerges at high fields and leads to splitting of the NMR central peak by alternating positive and negative hyperfine fields, as shown at 2.1 and 2.4 GPa in Fig. 4, A and B, respectively, both at $T = 0.07$ K. The sudden rise with field of the peak-splitting $f_R - f_L$ (a proxy AFM order parameter), shown in Fig. 4C, signals a discontinuous onset of AFM order at $H_C(P)$, with the discontinuity much weaker at the higher pressure.

In the AFM state, the uniform magnetization does not exhibit any obvious discontinuity at $H_C$ and remains < 2% of the saturated moment at our highest field of 15 T (fig. S5). A crossover temperature $T^*$ persists also at high fields, where the PS liquid develops increasing spin fluctuations (discussed further below).

### Spin-lattice relaxation rate

$1/T_1$ is a direct probe of low-energy spin fluctuations and can detect the PS and AFM transitions more precisely than the line shifts; the two probes give consistent results. Figure 5, A and B, show $1/T_1$ at $P = 2.1$ GPa for a wide range of applied fields that we grouped into those below and >6.2 T, corresponding, respectively, to the low-$T$ PS and AFM phases; Fig. 5, C and D, show the same at 2.4 GPa with the separation at 5.8 T.

At 2.1 GPa (Fig. 5B), we found a sharp drop of $1/T_1$ at $T^* \simeq 3$ to 4 K and a broad peak or sharper kink <2 K. At low fields in Fig. 5A, the latter feature appeared up to 6.1 T and clearly marked the opening of a spin gap below $T_P$. At $P = 2.4$ GPa, we did not find a peak at $T_P$ (Fig. 5C), but rather a sharp crossover from a low-$T$ gapped regime to a window with power-law behavior that is analyzed in Fig. 5E and will be further discussed below. At the higher fields in Fig. 5, B and D, the low-$T$ features (<0.8 K) are much sharper and coincide with the NMR peak splitting in Fig. 4, A and B. Thus, we can safely identify these peaks for $H \geq 6.33$ T as $T_N$ (*37*). The minimum in $1/T_1$ around 1.5 K in Fig. 5B increases with the field, indicating increasing spin fluctuations in the PS liquid state.

Figure 5F shows very clear field-induced PS-AFM transitions revealed by these signals at both $P = 2.1$ and 2.4 GPa. The PS and AFM boundaries, $T_P(H)$ and $T_N(H)$, respectively, meet at a very low $T_C$. Given phase coexistence (Fig. 4, A and B), the QPT at $H_C$ is clearly first order. The proxy AFM order parameter $f_R - f_L$ in Fig. 4C is consistent with $H_C$ determined from $1/T_1$ at both pressures. The much smaller first-order discontinuity of $f_R - f_L$ at the higher pressure indicates the approach toward a continuous QPT.

We extracted the PS spin gap $\Delta$ by fitting $1/T_1$ below $T_P$ to a semi-empirical form $T^{-a}e^{-\Delta/k_BT}$ with $a \approx 1$ [see section S5 of the supplementary materials (*33*)]. As expected, a linear decrease with $H$ of $\Delta$ at both pressures is revealed in Fig. 6A and is caused by the field lowering of the $S = 1$ ($S^z = 1$) state above the singlet PS ground state. These results are compatible with previously determined $H = 0$ gap estimates (*29*, *30*) and the known $g$ factor.

At a first-order transition into the AFM phase, the PS gap should jump discontinuously

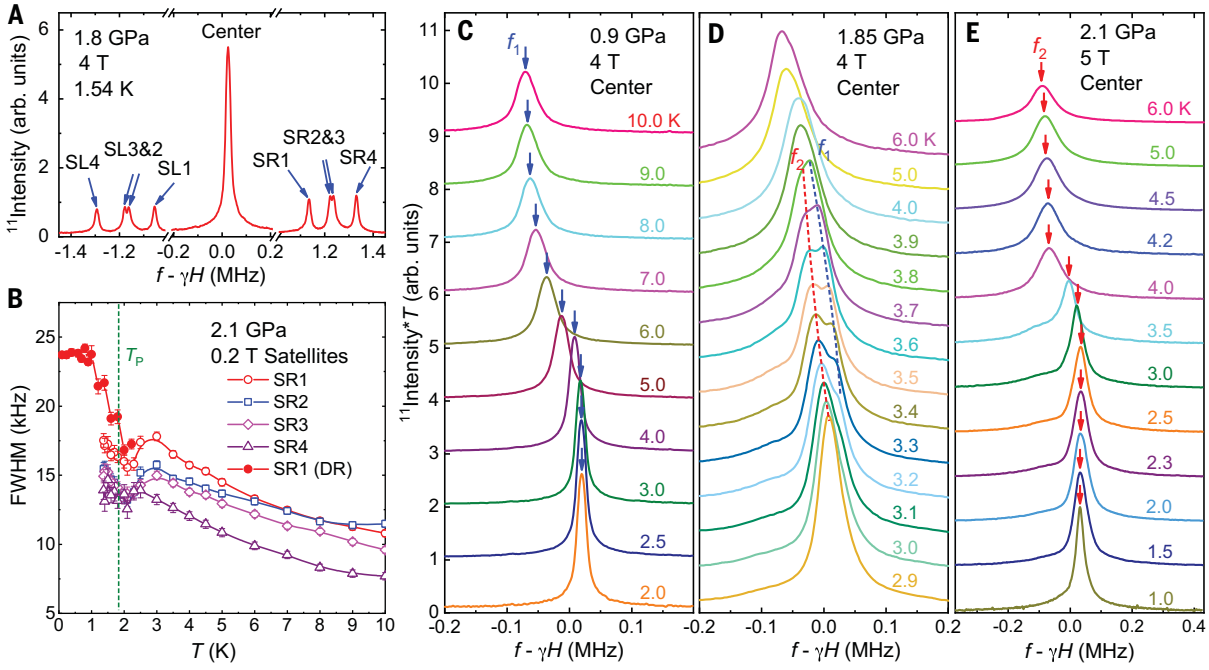


**Fig. 3. NMR spectra and line shifts.** (**A**) NMR $^{11}$B spectrum at $H$ = 4 T and $P$ = 1.8 GPa, with the field applied at 8.6° from the crystalline $c$ axis, showing the center line and two sets of satellites associated with the four B sites (Fig. 1A). (**B**) FWHM of satellites SR1 to SR4 shown as a function of temperature at $P$ = 2.1 GPa and $H$ = 0.2 T. The line at 1.8 K marks the onset of an upturn with further cooling. SR1 was measured in the dilution refrigerator in addition to the regular helium cryostat used for all cases [see section S2 of the supplementary materials (*33*)]. (**C** to **E**) NMR center line for a range of temperatures (curves shifted vertically for clarity) at $P$ = 0.9 GPa and $H$ = 4 T (C), 1.85 GPa and 4 T (D), and 2.1 GPa and 5 T (E). The peaks in the DS phase (C) and in and above the PS phase (E) are marked $f_1$ and $f_2$, respectively. The split peak in (D) reflects phase coexistence.

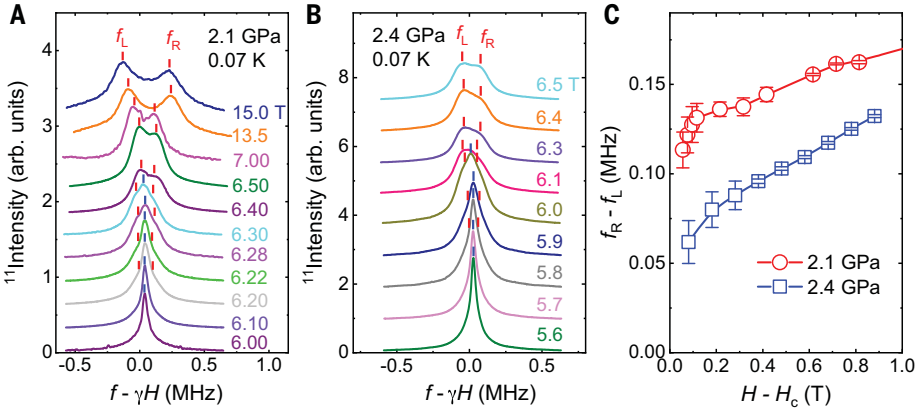


**Fig. 4. AFM transition.** Splitting of the NMR center line with increasing $H$ at $T$ = 0.07 K is shown in (**A**) and (**B**) for $P$ = 2.1 and 2.4 GPa, respectively. The two peaks marked $f_L$ and $f_R$ (red bars) indicate AFM order developing above $H \simeq 6$ T. A center peak (blue bars) remaining at fields up to 6.1 T indicates phase coexistence. (**C**) Proxy AFM order parameter $f_R - f_L$ versus $H - H_C$, where $H_C$ is determined using the spin-lattice relaxation rate (Fig. 5).

to zero at $H_C$ (given that the AFM state is gapless), but despite the clear first-order signals described above (Fig. 4C), we found that $\Delta(H_C)$ values were indistinguishable from zero within statistical errors. We will discuss the anomalously small gap discontinuity in the context of the proximate DQCP scenario further below.

### Deconfined quantum criticality

The SSM at $H$ = 0 has been a candidate for a DQCP separating its coupling-induced PS and AFM ground states (*7*, *38*). The singlets in the PS phase of the model occupy the empty plaquettes, in contrast to the FP state in $SrCu_2(BO_3)_2$ (Fig. 1B). This aspect of the PS state depends sensitively on other possible weak interactions beyond the SSM (*11*, *39*), and the SSM description of the global phase diagram of $SrCu_2(BO_3)_2$ should remain valid.

There is mounting theoretical evidence that a gapless QSL phase can exist between a PS state (or closely related spontaneously dimerized state) and the AFM state in frustrated 2D quantum spin systems (*16*, *20*, *40*–*42*) and that these QSL phases generically end at multicritical DQCPs (*15*, *17*, *18*). Beyond such a point, the transition without intervening QSL is expected to be first order, with the coexistence state at $H$ = 0 inheriting (and breaking) the emergent O(4) or SO(5) symmetry, depending on the type of singlet-ordered phase (*7*, *8*, *10*, *12*, *13*) of the DQCP.

In the $H$ = 0 SSM, early calculations indicated a first-order PS-AFM transition (*27*), and a recent calculation suggested an O(4) [from the O(3) AFM and scalar PS order parameters] multicritical DQCP in an extended parameter space (*11*). A generic O(4) DQCP had previously been proposed (*38*). The intervening gapless QSL between the PS and AFM phases was identified very recently (*17*, *19*) and may be explained by an instability of the conventional DQCP (*15*). These theoretical insights, along with our NMR results for $SrCu_2(BO_3)_2$, suggest the scenario in Fig. 2. Because no experiment so far (including ours) has explicitly confirmed a QSL phase, the possibility remains that there is instead

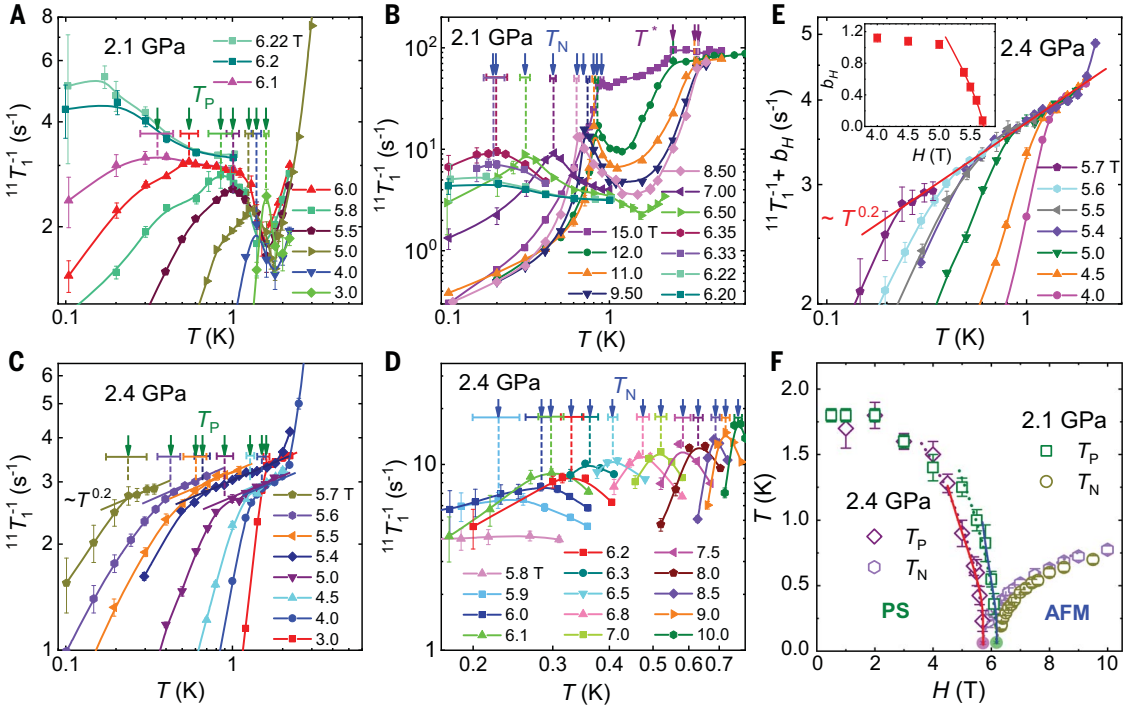


**Fig. 5. Spin-lattice relaxation.** $1/^{11}T_1(T)$ was measured at 2.1 GPa [(**A**) and (**B**)] and 2.4 GPa [(**C**) and (**D**)], which are separated to show the PS [(A) and (C)] and AFM [(B) and (D)] states. The drop in $1/T_1$ at a $T^* \simeq 4$ K [(A) and (B)] indicates the sharp crossover into the PS liquid. The peaks at lower $T$ mark $T_P$ and $T_N$, with uncertainties indicated by the horizontal bars. At 2.4 GPa, no low-$T$ PS peak is observed (C), but $T_P$ can be extracted from the sudden change from thermally activated to quantum critical behavior, $1/T_1 = aT^\eta - b_H$. (**E**) Inset: Power-law scaling of the offset, $b_H \propto (H_C - H)^d$ with $d \approx 0.8$, close to $H_C$. Main panel: The common scaling form with constant $a$ and $\eta \approx 0.2$ is demonstrated, and $b_H$ has been added. (**F**) Low-temperature phase diagrams at 2.1 and 2.4 GPa. The solid and dotted lines indicate the phase boundaries modeled by, respectively, a logarithmic form of $T_P$ and near-critical forms of both $T_P$ and $T_N$ [see section S6 of the supplementary materials (*33*)]. The latter fits give the $T_C$ values indicated with circles.

another line of PS–AFM transitions. Although the dashed regions in the phase diagrams in Fig. 2 can represent either possibility, specific heat measurements at $H = 0$ (*30*, *31*) found no phase transition between 2.6 and 3.2 GPa, consistent with a QSL ground state evolving into the $T > 0$ PS liquid.

A putative multicritical DQCP at $H > 0$ should evolve from a corresponding $H = 0$ DQCP with emergent O(4) symmetry (*7*, *38*). Although this O(4) point exists only in an extended parameter space outside of the ($g$, $H$, $T$) cube in Fig. 2, the fact that the field-induced magnetization is very small at $H_C$ [see section S4 of the supplementary materials (*33*)] suggests that the putative $H > 0$ DQCP still hosts an approximate O(4) symmetry, with stronger O(3) character developing on the first-order line. Strictly speaking, at $H > 0$, the DQCP may evolve into a near-critical triple point with first-order signatures at the lowest energy scales.

Closer proximity of $SrCu_2(BO_3)_2$ to some continuous QPT with increasing pressure is certainly supported by our observation of a weaker discontinuity of the AFM order parameter at 2.4 GPa than at 2.1 GPa (Fig. 4C). Moreover, at a clearly first-order transition, correspondingly high $T_C$ values would normally be expected. The low $T_C$ at both pressures then point to a mechanism suppressing long-range order rather far away from the QPT. The DQCP scenario offers this possibility through its emergent continuous symmetry inherited (at least up to some large length scale) by the first-order line. An ideal 2D coexistence state with continuous order parameter symmetry must have $T_C = 0$, but weak violations of the symmetry [in combination with 3D effects (*43*)] would imply a low $T_C > 0$, as observed in $SrCu_2(BO_3)_2$.

In the scenario of a first-order transition with emergent O(3) symmetry, the Ising-type PS order can be understood as an uniaxial deformation of the O(3) order parameter. A logarithmic form of the PS transition temperature is then expected: $T_P \propto \ln^{-1}[a(H_C - H)]$ for some value of $a$ (*7*, *44*). Fits of the experimental data to this form [see section S6 of the supplementary materials (*33*)] are shown with solid curves in Fig. 5F and indeed describe the behavior close to $H_C$.

To describe $T_N(H)$, we note again that interlayer interactions are required for $T_N > 0$ in a spin-isotropic system. These 3D couplings also change a continuous QPT ($T_C = 0$) into a first-order line extending to a bicritical or triple point at $T_C > 0$ (*38*, *43*) (red crosses in Fig. 2B). Given the extremely low $T_C$ values in $SrCu_2(BO_3)_2$, a modified critical form with the same exponent $\phi$ governing both transitions above $T_C$ may be expected from DQCP dualities (*13*, *45*): $T_{P,N} = T_C + a_{P,N}|H - H_C|^\phi$. Fits with independent exponents $\phi$ for the PS and AFM transitions [see section S6 of the supplementary materials (*33*)] indeed support a common value and motivate joint fitting with a single $\phi$. Such fits are shown by the dashed curves in Fig. 5, where $T_C$ is in the range of 0.05 to 0.07 K at both pressures. At 2.1 GPa, $H_C = 6.183 \pm 0.007$ and $\phi = 0.57 \pm 0.02$, and at 2.4 GPa, $H_C = 5.719 \pm 0.007$ and $\phi = 0.50 \pm 0.04$. These fits in which $\phi$ is close to estimates for both SO(5) (*12*, *14*) and O(4) (*45*) DQCPs [see section S6A of the supplementary materials (*33*)] do not rule out the alternative logarithmic form of $T_P$ but do further validate the very low $T_C$ values and common transition field $H_C$ for both order parameters.

### Quantum-critical relaxation

As shown in Fig. 5C, $1/T_1$ at 2.4 GPa exhibits $T^\eta$ scaling with $\eta \approx 0.2$ within a window of temperatures for several fields close to $H_C$ on the PS side. The ensemble of fits is further analyzed in Fig. 5E using the expected quantum-critical form $1/T_1 = aT^\eta - b_H$ (*46*), where $a$ is a constant and $b_H > 0$ for $H < H_C$. The fact that scaling behavior is not observed at 2.1 GPa (Fig. 5A) suggests that only the system at 2.4 GPa is sufficiently close to a continuous QPT that it realizes the quantum critical fan (*46*). This is depicted in Fig. 2B, where $T$ is the largest energy scale (but low enough so that the correlation length is well above the lattice constant). The value of $\eta$ is compatible with an estimate for an O(4) DQCP (*45*) and slightly below the SO(5) value (*2*, *12*).

On the AFM side (Fig. 5D), $1/T_1$ is dominated by the 3D effects causing $T > 0$ AFM order, with

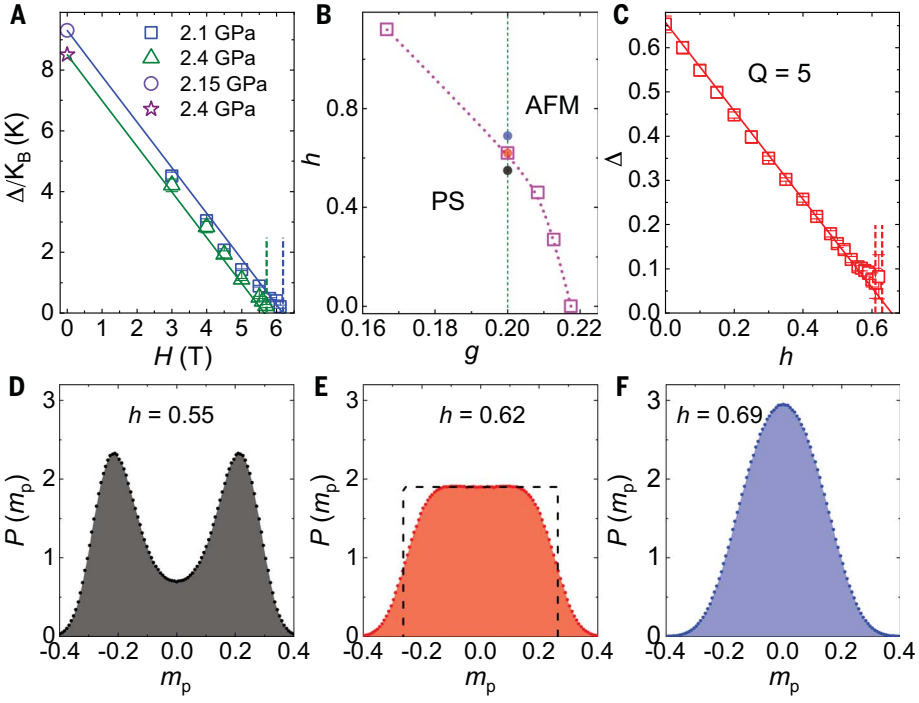


**Fig. 6. Spin gap and emergent symmetry.** (**A**) Field-dependent gap of $SrCu_2(BO_3)_2$ from experimental data. The lines show the expected form $\Delta(H) = \Delta(0) - \tilde{g}\mu_B H$, where $\Delta(0)$ represents the reported zero-field gaps with pressure at 2.15 GPa (*29*) and 2.4 GPa (*30*), and $\tilde{g} = 2.28$ is the known $g$ factor [see section S5 of the supplementary materials (*33*)]. The vertical dashed lines represent $H_C$ values from Fig. 5F. (**B**) Calculated ground-state phase diagram of the CBJQM versus $g = J/Q$ and field $h$. The PS and AFM phases are separated by a first-order transition. The vertical line and closely spaced points mark the parameters in (D) to (F). (**C**) Calculated spin gap of the CBJQM at $g = 0.2$. The dashed vertical line indicates $h_C$, and the solid line is a fit to $\Delta(h) = \Delta(0) - h$. (**D** to **F**) Calculated distribution of the plaquette order parameter. Double-peak (D), plateau (E), and single-peak (F) distributions are found, respectively, in the PS phase ($h = 0.55$), at the transition ($h = 0.62$), and in the AFM phase ($h = 0.69$).

the associated peak in $1/T_1$ masking any 2D quantum criticality, unlike the PS side, where the spin correlations and 3D effects are much weaker. We lack 2.4 GPa data at temperatures higher than those shown in Fig. 5C. At 2.1 GPa, no scaling is observed between $T_N$ and $T^*$ in Fig. 5B, where a sharp drop below $T^*$ is immediately followed by strong precursors to AFM ordering.

### Quantum spin model

We now turn to the checkerboard $J - Q$ model (CBJQM), in which four-spin interactions $Q$ replace $J'$ in the SSM. The CBJQM is amenable to quantum Monte Carlo simulations and hosts PS and AFM phases separated by a first-order transition with emergent O(4) symmetry at zero field (*7*). We here simulate [see section S1 of the supplementary materials (*33*)] the same model in a field, defining $g = J/Q$ and $h = H/J$ with $J = 1$.

In the phase diagram in Fig. 6B, the field-driven PS-AFM transition is first order. The PS gap $\Delta(h)$ obtained from the low-temperature susceptibility (fig. S22) is shown in Fig. 6C at $g = 0.2$, below the $h = 0$ transition at $g_C(0) \approx 0.217$. The expected linear form $\Delta(h) = \Delta(0) - h$ for an $S^z = 1$ excitation is observed for $h < h_C$, with $h_C$ slightly less than $\Delta(0)$, implying a small gap discontinuity at $h_C$. We also observed a very small magnetization jump, ~0.002 per spin. These behaviors are reminiscent of the well-known "spin-flop" transitions from Ising to canted XY AFM phases, but with anomalously small magnetization discontinuity. In section S8 of the supplementary materials (*33*), we posit that the small magnetization and gap discontinuities, which decrease further upon moving closer to $g_C(0)$, reflect an approximate emergent O(3) symmetry in the CBJQM at $h > 0$.

The emergent symmetry can also be studied directly. At $h = 0$, the O(3) AFM order parameter $(m_x,m_y,m_z)$ combines with the scalar PS order parameter $m_p$ into an O(4) vector $(m_x,m_y,m_z,m_p)$ at the $T = 0$ transition (*7*, *43*). To detect the putative O(3) symmetry of $(m_x, m_y,m_p)$ at $h > 0$, we studied the distribution $P(m_p)$ along the vertical line in Fig. 6B. In the PS phase (Fig. 6D), $P(m_p)$ exhibits the expected double peak, reflecting the $Z_2$ symmetry that is broken in the thermodynamic limit. In the AFM phase (Fig. 6F), there is a single central peak, reflecting the lack of PS order.

At a conventional first-order transition, a three-peak distribution would follow from coexisting PS and AFM orders. By contrast, the distribution in the coexistence state in Fig. 6E is nearly uniform over a range of $m_p$ values (with finite-size rounded edges). The distribution $P(m_p)$ obtained by integrating an O(3) symmetric $P(m_p,m_x,m_y)$ over $m_x$ and $m_y$ should indeed be uniform for $m_p \in [-R,R]$, where $R \equiv \max(|m_p|)$; therefore, the approximately flat distribution demonstrates emergent O(3) symmetry in the presence of finite-size fluctuations of $R$. Although this symmetry cannot be exact, i.e., it exists up to some finite length scale, it is responsible for suppressing $T_C$ and the gap at $H_C$; see fig. S19, where we also show supporting results for cross-correlations between the PS and AFM order parameters.

We expect the same O(3) emergent symmetry at the PS-AFM transition in $SrCu_2(BO_3)_2$, in which the ordered coexistence state breaks the symmetry. The symmetry should be violated on long length scales because of the distance to the DQCP and also by 3D couplings. One of the Goldstone modes associated with the coexistence state then develops a small gap. Studies of the CBJQM with interlayer couplings suggest that the symmetry is unexpectedly robust (*43*).

Emergent O(3) symmetry on large length scales in $SrCu_2(BO_3)_2$ is supported, in particular, by our results at 2.1 GPa, where Fig. 4C shows a large discontinuity in the AFM order parameter, but $T_C$ is low and the gap (Fig. 6A) is very small at $H_C$. Moreover, the uniform magnetization is extremely small and does not exhibit a discernible discontinuity (fig. S5). These behaviors are analogous to those in the CBJQM for $g$ close to $g_C(0)$.

### Discussion

Our high-pressure NMR experiments on $SrCu_2(BO_3)_2$ in a magnetic field establish an example of a quantum magnet realizing DQCP phenomenology, which thus far had existed only in the realm of field theories and model studies. We have demonstrated PS and AFM transitions, with $T_P(H)$ and $T_N(H)$ merging at $T_C \simeq 0.07$ K and $H_C \simeq 6$ T. The PS-AFM transition at $H_C$ is first order, with discontinuity weakening with increasing pressure.

We have argued that the suppression of $T_C$ and absence of statistically significant PS gap discontinuity are consequences of emergent O(3) symmetry generated by a nearby DQCP. At the highest pressure, 2.4 GPa, $1/T_1$ exhibits critical scaling for $T$ between 0.2 and 2 K, indicating sufficient proximity to the DQCP [which is likely of the multicritical type (*14*, *15*, *17*, *18*)] for realizing the characteristic quantum-critical fan (*46*) on the gapped PS side

of the transition. Strong 3D AFM ordering effects on the gapless side of the transition mask putative quantum criticality in $1/T_1$ there, but the AFM ordering temperature $T_N$ vanishes in a way very similar to the PS ordering temperature $T_P$, again in support of emergent symmetry of the order parameters.

The $H = 0$ AFM phase was previously detected in the specific heat between 3.2 and 4 GPa (*30*), with $T_N$ from 2 to 3.5 K. Subsequently, results at $H > 0$ were also reported (*31*). However, whereas $T_P(H)$ from the specific heat agrees well with our PS transitions shown in Fig. 1D, the heat capacity peak assumed to signal the AFM transition did not drop below 1 K (*31*), extending above the PS phase at fields as low as 3 T. It may be difficult to detect the small specific-heat peak signaling the AFM transition (*30*) in high-field measurements at low temperatures.

Beyond the highest pressure reached here, a plausible scenario (*15*, *17*) is a QSL between the PS and AFM phases (Fig. 2). Our experiments do not directly address the putative QSL, and further investigations should elucidate the low-$T$, $H = 0$ state between 2.6 and 3 GPa [where no order has been detected (*30*, *31*)] and its evolution as $H$ approaches 5.7 T, where our current experiments point to a DQCP slightly above 2.4 GPa.

## REFERENCES AND NOTES


1. T. Senthil, A. Vishwanath, L. Balents, S. Sachdev, M. P. A. Fisher, *Science* **303**, 1490–1494 (2004).
2. A. W. Sandvik, *Phys. Rev. Lett.* **98**, 227202 (2007).
3. T. Senthil, L. Balents, S. Sachdev, A. Vishwanath, M. P. A. Fisher, *Phys. Rev. B* **70**, 144407 (2004).
4. H. Shao, W. Guo, A. W. Sandvik, *Science* **352**, 213–216 (2016).
5. N. Ma *et al*., *Phys. Rev. B* **98**, 174421 (2018).
6. A. Nahum, P. Serna, J. T. Chalker, M. Ortuño, A. M. Somoza, *Phys. Rev. Lett.* **115**, 267203 (2015).
7. B. Zhao, P. Weinberg, A. W. Sandvik, *Nat. Phys.* **15**, 678–682 (2019).
8. P. Serna, A. Nahum, *Phys. Rev. B* **99**, 195110 (2019).
9. G. J. Sreejith, S. Powell, A. Nahum, *Phys. Rev. Lett.* **122**, 080601 (2019).
10. J. Takahashi, A. W. Sandvik, *Phys. Rev. Res.* **2**, 033459 (2020).
11. N. Xi, H. Chen, Z. Y. Xie, R. Yu, arXiv:2111.07368 [cond-mat.str-el] (2021).
12. A. Nahum, J. T. Chalker, P. Serna, M. Ortuño, A. M. Somoza, *Phys. Rev. X* **5**, 041048 (2015).
13. C. Wang, A. Nahum, M. A. Metlitski, C. Xu, T. Senthil, *Phys. Rev. X* **7**, 031051 (2017).
14. B. Zhao, J. Takahashi, A. W. Sandvik, *Phys. Rev. Lett.* **125**, 257204 (2020).
15. D.-C. Lu, C. Xu, Y.-Z. You, *Phys. Rev. B* **104**, 205142 (2021).
16. W.-Y. Liu *et al*., *Sci. Bull.* **67**, 1034–1041 (2022).
17. J. Yang, A. W. Sandvik, L. Wang, *Phys. Rev. B* **105**, L060409 (2022).
18. W.-Y. Liu *et al*., *Phys. Rev. X* **12**, 031039 (2022).
19. A. Keleş, E. Zhao, *Phys. Rev. B* **105**, L041115 (2022).
20. H. Shackleton, A. Thomson, S. Sachdev, *Phys. Rev. B* **104**, 045110 (2021).
21. Y.-H. Zhang, S. Sachdev, *Phys. Rev. B* **102**, 155124 (2020).
22. H. Kageyama *et al*., *Phys. Rev. Lett.* **82**, 3168–3171 (1999).
23. S. Miyahara, K. Ueda, *Phys. Rev. Lett.* **82**, 3701–3704 (1999).
24. S. Miyahara, K. Ueda, *J. Phys.* **15**, R327–R366 (2003).
25. B. S. Shastry, B. Sutherland, *Physica B+C* **108**, 1069–1070 (1981).
26. A. Koga, N. Kawakami, *Phys. Rev. Lett.* **84**, 4461–4464 (2000).
27. P. Corboz, F. Mila, *Phys. Rev. B* **87**, 115144 (2013).
28. S. Haravifard *et al*., *Nat. Commun.* **7**, 11956 (2016).
29. M. E. Zayed *et al*., *Nat. Phys.* **13**, 962–966 (2017).
30. J. Guo *et al*., *Phys. Rev. Lett.* **124**, 206602 (2020).
31. J. L. Jiménez *et al*., *Nature* **592**, 370–375 (2021).
32. Y. H. Matsuda *et al*., *Phys. Rev. Lett.* **111**, 137204 (2013).
33. Materials and methods, additional NMR data, data analysis, and supporting theoretical results are available as supplementary materials.
34. K. Kodama *et al*., *J. Phys.* **14**, L319 (2002).
35. T. Waki *et al*., *J. Phys. Soc. Jpn.* **76**, 073710 (2007).
36. M. Takigawa, T. Waki, M. Horvatić, C. Berthier, *J. Phys. Soc. Jpn.* **79**, 011005 (2010).
37. T. Moriya, *J. Phys. Soc. Jpn.* **18**, 516–520 (1963).
38. J. Y. Lee, Y.-Z. You, S. Sachdev, A. Vishwanath, *Phys. Rev. X* **9**, 041037 (2019).
39. C. Boos *et al*., *Phys. Rev. B* **100**, 140413 (2019).
40. S.-S. Gong, W. Zhu, D. N. Sheng, O. I. Motrunich, M. P. A. Fisher, *Phys. Rev. Lett.* **113**, 027201 (2014).
41. L. Wang, A. W. Sandvik, *Phys. Rev. Lett.* **121**, 107202 (2018).
42. Y. Nomura, M. Imada, *Phys. Rev. X* **11**, 031034 (2021).
43. G. Sun, N. Ma, B. Zhao, A. W. Sandvik, Z. Y. Meng, *Chin. Phys. B* **30**, 067505 (2021).
44. V. Y. Irkhin, A. A. Katanin, *Phys. Rev. B* **57**, 379–391 (1998).
45. Y. Q. Qin *et al*., *Phys. Rev. X* **7**, 031052 (2017).
46. A. V. Chubukov, S. Sachdev, J. Ye, *Phys. Rev. B* **49**, 11919–11961 (1994).
47. Y. Cui *et al*., Data and simulation codes for: Proximate deconfined quantum critical point in $SrCu_2(BO_3)_2$, Zenodo (2023); https://doi.org/10.5281/zenodo.7600028.


## ACKNOWLEDGMENTS

We thank B. Normand for extensive suggestions and constructive criticism and W. Guo, F. Mila, M. Takigawa, Y. Wang, Z.-Y. Xie, and Y.-Z. You for helpful discussions. **Funding:** This work was supported by the Ministry of Science and Technology of China (grants 2022YFA1402700, 2022YFA1403402, and 2021YFA1400401), the National Natural Science Foundation of China (grants 12134020, 12104503, 12174441, and 51872328), the Simons Foundation (investigator grant 511064), the Strategic Priority Research Program(B) of the Chinese Academy of Sciences (grant XDB33010100), the K. C. Wong Education Foundation (grant GJTD2020-01), the Beijing Institute of Technology Research Fund Program for Young Scholars, the Fundamental Research Funds for the Central Universities, and the Research Funds of Renmin University of China (grants 22XNH096 and 21XNLG18). Some of the numerical calculations were performed on the Shared Computing Cluster managed by Boston University's Research Computing Services. Part of the measurements were conducted at the Cubic Anvil Cell Station, the Synergetic Extreme Condition User Facility (SECUF). **Author contributions:** Y.C. performed NMR measurements and data analysis with assistance from C.L., Z.H., and W.Y.. W.H. and S.L. provided single crystals. X.L. and H.L. performed the Bayesian fitting analysis. L.L., H.L., N.X., and K.H.W. performed numerical simulations with guidance from R.Y. and A.W.S.. W.Y., A.W.S., and R.Y. guided the project and wrote the manuscript with input from all authors. **Competing interests:** The authors declare no competing interests. **Data and materials availability:** The data and simulation codes needed to evaluate the conclusions in this study have been deposited at Zenodo (*47*).


## SUPPLEMENTARY MATERIALS

science.org/doi/10.1126/science.adc9487
Materials and Methods
Figs. S1 to S22
Table S1
References (*48*–*65*)

Submitted 10 May 2022; accepted 12 May 2023
10.1126/science.adc9487

# Proximate deconfined quantum critical point in $SrCu_2(BO_3)_2$

Yi Cui, Lu Liu, Huihang Lin, Kai-Hsin Wu, Wenshan Hong, Xuefei Liu, Cong Li, Ze Hu, Ning Xi, Shiliang Li, Rong Yu, Anders W. Sandvik, and Weiqiang Yu

*Science*, **380** (6650), .
DOI: 10.1126/science.adc9487

**Editor's summary**
Transitions between phases with unrelated symmetries are expected to be discontinuous. Nearly two decades ago, a different, continuous kind of transition between such phases was proposed under the name deconfined quantum critical point (DQCP). However, observing the DQCP experimentally has proven to be extremely challenging. Cui *et al*. used nuclear magnetic resonance to study the magnetic field–driven transitions of the layered material $SrCu_2(BO_3)_2$ at various pressures. At high pressures, the experimental results combined with numerical calculations pointed to the existence of a nearby DQCP. —Jelena Stajic